

Optically Mediated Hybridization Between Two Mechanical Modes

A. B. Shkarin,^{1,*} N. E. Flowers-Jacobs,¹ S. W. Hoch,¹ C. Deutsch,² J. Reichel,² and J. G. E. Harris^{1,3}

¹*Department of Physics, Yale University, New Haven, CT 06520, USA*

²*Laboratoire Kastler Brossel, ENS/UPMC-Paris 6/CNRS, F-75005 Paris, France*

³*Department of Applied Physics, Yale University, New Haven, CT 06520, USA*

(Dated: June 12, 2025)

In this paper we study a system consisting of two nearly degenerate mechanical modes that couple to a single mode of an optical cavity. We show that this coupling leads to nearly complete (99.5%) hybridization of the two mechanical modes into a bright mode that experiences strong optomechanical interactions and a dark mode that experiences almost no optomechanical interactions. We use this hybridization to transfer energy between the mechanical modes with 40% efficiency.

PACS numbers: 42.50.Wk, 42.81.Wg, 42.60.Da, 85.85.+j, 03.67.-a

Optomechanical systems, in which electromagnetic resonators interact with mechanical resonators, offer a platform for studying a wide range of nonlinear and quantum effects. These systems have been studied in the context of quantum-limited detection of forces and displacements, the production of nonclassical states of light, synchronization and chaotic dynamics, and tests of quantum mechanics with massive degrees of freedom.[1]

Optomechanical systems are usually modeled as a single optical mode that is parametrically coupled to a single mechanical mode. This simple model accurately describes many experiments; however, real devices invariably consist of multiple optical and mechanical modes. The presence of multiple modes can provide important capabilities, including new types of optomechanical interactions, robust means for detecting quantum effects, and the transfer of quantum states between different systems.[2–11]

One important class of multimode optomechanical systems consists of devices in which a single optical mode couples to multiple mechanical modes. This situation arises naturally when an optomechanical device with well-separated optical resonances is driven by a single laser beam. Within the usual weak-coupling description of optomechanics the undriven optical modes are irrelevant, and only the driven mode needs to be considered.[12–14] Mechanical modes, on the other hand, cannot be ignored just because they are not driven. This is because any optical mode can be detuned (to some degree) by the displacement of any of the devices' mechanical modes. As a result the effective Hamiltonian for such a device will involve one optical mode coupled to many mechanical modes.

In such a system, the motion of a given mechanical mode will modulate the intracavity optical field, which will in turn drive the other mechanical modes. This can be thought of as an optically mediated coupling between the mechanical modes. This intermode coupling can be neglected for mechanical modes whose resonance frequencies are well separated. However, mechanical resonators with

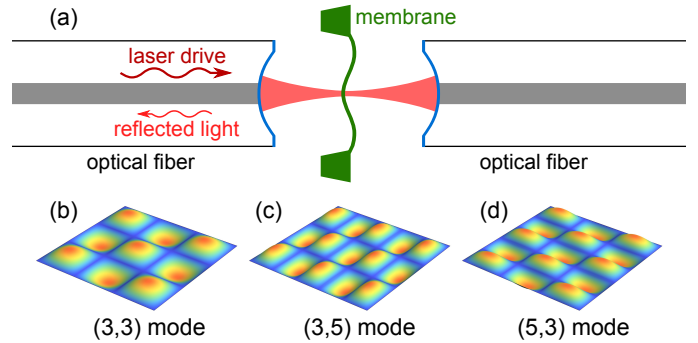


FIG. 1. (a): Experimental setup with a SiN membrane placed in a cavity formed between the mirrored ends of two fibers. (b)-(d): Schematic representation of the mode shapes of the three relevant membrane modes.

some degree of symmetry will have some nearly degenerate modes, and for these modes this coupling can be important.

In this paper we demonstrate that the coupling between one optical mode and two mechanical modes causes the mechanical modes to hybridize into bright and dark states. While previous experiments have demonstrated the optomechanical hybridization of mechanical modes[15–17], the results presented here have a number of novel features. First, the mechanical modes couple to each other only via the optical mode; second, the hybridization between the modes is nearly complete; and third, we demonstrate the transfer of mechanical energy between the modes by modulating the hybridization. We find that these results are consistent with a straightforward extension of the usual optomechanical equations of motion to include multiple mechanical modes.

The device described here operates in the classical regime. However, in the quantum regime (that is, when the mechanical modes are nearly in the ground state) the fact that the intermode coupling is both conservative and strong (in contrast to previous work [15–17]) means that it would be well-suited for realizing proposals for entangling mechanical modes and creating non-classical mechan-

* alexey.shkarin@yale.edu

ical states[4, 7, 9]. In addition, the long lifetime of the mechanically dark state can also be used to store quantum information[15, 18].

The device studied here is a “membrane-in-the-middle” optomechanical system composed of a SiN membrane placed in an optical fiber-cavity (Fig. 1a)[19, 20]. The 70 μm long Fabry-Perot cavity is formed between the end faces of two 200 μm diameter single-mode optical fibers. Each fiber face has a Gaussian-shaped concavity with a 300 μm radius of curvature and a dielectric coating that is highly reflective at wavelength $\lambda = 1550$ nm. The resulting cavity has a finesse $\lesssim 100,000$ depending upon the position of the membrane, corresponding to a cavity linewidth $\kappa/2\pi \gtrsim 20$ MHz.

The SiN membrane is 250 μm square and 100 nm thick. Because it is nearly square and under significant stress, the resonance frequencies of its higher-order modes are expected to be simply related to its fundamental resonance frequency $\omega_{(1,1)}/2\pi = 1.7$ MHz. Labeling each mode by the number of anti-nodes along each axis (j, k), as shown in Fig. 1, the resonance frequencies are $\omega_{(j,k)} = \omega_{(1,1)}\sqrt{j^2 + k^2}/\sqrt{2}$. We find that the measured $\omega_{(j,k)}$ follow this relationship to within 0.1% for $j, k < 6$, implying that each mode with $j \neq k$ has a (nearly) degenerate partner.

As described in [20], the membrane is positioned so that the frequency of the optical cavity varies linearly with the membrane position. The cavity is locked to the laser at frequencies $\ll \omega_{(1,1)}$ so the membrane’s motion is imprinted on the reflected laser field, which is measured using a heterodyne technique. We measure the power spectral density of the heterodyne signal near the membrane’s resonance frequencies and fit this data to extract each mechanical mode’s linewidth and resonance frequency.

Before concentrating on the cavity-induced coupling between nearly degenerate mechanical modes, we characterize the optomechanical shift in the resonance frequency (“optical spring”) and linewidth (“optical damping”) of the non-degenerate (3,3) mode. For this mode, $\omega_{(3,3)}/2\pi = 5.092$ MHz, the quality factor $Q_{(3,3)} = 500,000$, and the single-photon optomechanical coupling $g_{(3,3)}/2\pi = 1050$ Hz. The effective mass is $m = 5.4$ ng, which is the same for all of the membrane’s modes.

The effects of the optomechanical coupling are revealed by varying the detuning Δ between the laser and the cavity. In Fig. 2 we plot the shift in the mechanical linewidth $\delta\gamma_{(3,3)}$ and the resonance frequency $\delta\omega_{(3,3)}$ as a function of Δ . Since $\omega_{(3,3)} \approx 0.2\kappa$ (the unresolved-sideband regime), $\delta\omega_{(3,3)}$ and $\delta\gamma_{(3,3)}$ are largest when $\Delta \approx -\kappa/3$. We fit the data in Fig. 2 to theoretical predictions [12, 13] using the incident power P_{in} and cavity linewidth κ as fitting parameters. The result of this fit is shown in Fig. 2 (green line) and gives $\kappa/2\pi = 21$ MHz and $P_{\text{in}} = 3$ μW , in agreement with independent measurements.

Now we focus on the effect of the optomechanical coupling on the nearly degenerate (3,5) and (5,3) mechan-

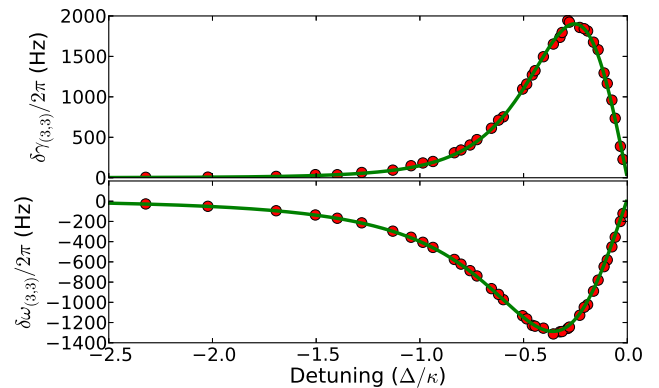


FIG. 2. Optomechanically-induced shift in mechanical linewidth (*top*) and frequency (*bottom*) of the (3,3) membrane mode as a function of detuning with theoretical fit (green line). This data is taken with an incident power of 3 μW and a cavity linewidth of 21 MHz.

ical modes. For these modes $\omega_{(3,5)}/2\pi = 6.999$ MHz, $\omega_{(5,3)}/2\pi = 7.005$ MHz, $Q_{(3,5)} = 440,000$, $Q_{(5,3)} = 220,000$, $g_{(3,5)}/2\pi = 700$ Hz, and $g_{(5,3)}/2\pi = 950$ Hz. In Fig. 3(a) we plot the measured power spectral density of the heterodyne signal as a function of Δ (*y*-axis) and the measurement frequency (*x*-axis).

When the laser power driving the cavity is relatively low ($P_{\text{in}} = 3$ μW) and the detuning $\Delta \ll -\kappa/3$ then the effect of the optomechanical coupling on the mechanical modes is minimal and the thermal motion of each mode is clearly visible in the power spectral density. For both modes, the optomechanical effects increase as Δ approaches $-\kappa/3$ and then decrease as Δ approaches 0. In Fig. 3(a) maximum optical spring is only ~ 1 kHz; since this is significantly smaller than the 5 kHz spacing between the two modes, the modes do not hybridize and instead independently exhibit essentially the same behavior as shown in Fig. 2 for the nondegenerate (3,3) mode.

On the other hand, in Fig. 3(c) the laser power $P_{\text{in}} = 38$ μW is large enough that at $\Delta \approx -1.5\kappa$ the shift in the mechanical resonance frequencies approaches the intrinsic mode spacing and single-mode optomechanics breaks down. As a result, the original mechanical modes hybridize into two new modes: a “bright” mode that exhibits strong optical spring and damping, and a “dark” mode that exhibits almost no optical spring or damping.

In order to make a quantitative comparison between the data in Fig. 3(a,c) and theory, we consider a system with several mechanical modes, all of which couple to a single optical mode. The optical mode’s linewidth is $\kappa = \kappa_{\text{L}} + \kappa_{\text{M}}$, where κ_{L} is the cavity loss rate due to coupling through the input mirror and κ_{M} includes all other losses. The cavity is driven by a laser with amplitude a_{in} which is detuned by Δ from the cavity resonant frequency ω_{c} . There are N mechanical oscillators coupled to the cavity mode and the n^{th} mechanical oscillator has a single-photon optome-

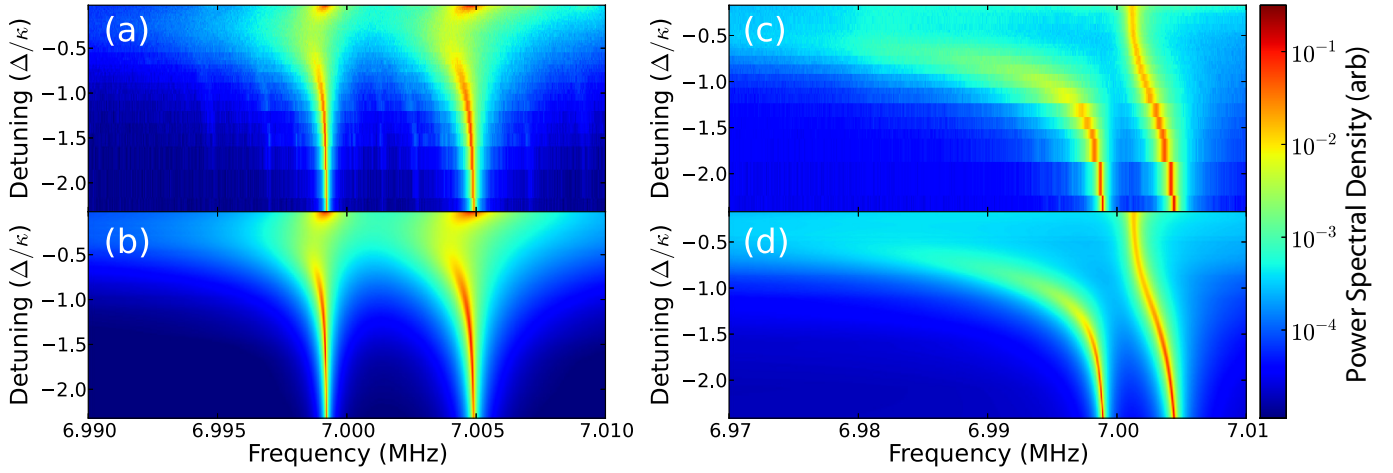


FIG. 3. Power spectral density of the heterodyne signal (a,c) and theoretical fits (b,d) as a function of measurement frequency (horizontal axis) and detuning between the incident laser and the cavity resonance (vertical axis). The data is presented for two incident laser powers: $3 \mu\text{W}$ for (a,b) and $38 \mu\text{W}$ for (c,d).

chanical coupling g_n , intrinsic linewidth γ_n , and resonant frequency ω_n . Since our room-temperature experiment is firmly in the classical regime $\hbar\omega_n \ll k_B T$, we use a classical analysis. We also disregard all noise on the optical drive. Under these assumptions, the system's linearized equations of motion are

$$\dot{d} = -\left(\frac{\kappa}{2} - i\Delta\right)d - i \sum_n \alpha_n z_n \quad (1)$$

$$\dot{c}_n = -\left(\frac{\gamma_n}{2} + i\omega_n\right)c_n - i(\alpha_n^* d + \alpha_n d^*) + \sqrt{\gamma_n} \eta_n, \quad (2)$$

where $d = a - \bar{a}$ are the small fluctuations of the optical mode's amplitude around its mean value $\bar{a} = \frac{\sqrt{\kappa_L a_{in}}}{\kappa/2 - i\Delta}$, $z_n = c_n^* + c_n$ is the position of the n^{th} mechanical oscillator, c_n is the quadrature amplitude of the mode's displacement, and $\alpha_n = \bar{a} g_n$. Each mode's thermal fluctuations are generated by a thermal Langevin force $\eta_n(t)$ where $\langle \eta_n(t) \eta_m(t') \rangle = \delta_{nm} \delta(t - t') k_B T / \hbar \omega_n$.

From this model, we can recover the standard dynamical backaction for a single mechanical mode coupled to a cavity[12, 13] by taking $N = 1$. To do this, we find the Fourier transform of the displacement $z_1[\omega]$ arising from the thermal Langevin force by inserting the expression for d from (1) into (2) and taking the limit $\omega_1 \gg \gamma_1$:

$$(\chi_1^{-1}[\omega] + i\Sigma_{11}[\omega])z[\omega] = \sqrt{\gamma_1} \eta_1[\omega] \quad (3)$$

where the intrinsic mechanical susceptibility $\chi_1[\omega]^{-1} = \gamma_1/2 - i(\omega - \omega_1)$ is modified by an optically-induced “self-energy” term $\Sigma_{11}[\omega] = -i|\alpha_1|^2(\chi_c[\omega] - \chi_c^*[-\omega])$ which is a function of the cavity susceptibility $\chi_c[\omega] = (\kappa/2 - i(\omega + \Delta))^{-1}$. This self-energy represents the optomechanical contribution to the mechanical resonance frequency $\delta\omega_1 = \text{Re}(\Sigma_{11}[\omega_1])$ and damping $\delta\gamma_1 = -2\text{Im}(\Sigma_{11}[\omega_1])$. The (3,3) mode data in Fig. 2 is fit to these expressions

for $\delta\omega_1$ and $\delta\gamma_1$, which are consistent with more complete derivations of single-mode dynamical backaction[12, 13].

Extending this approach to the full system with N oscillators coupled to a single cavity, the analog of (3) is

$$(\chi_n^{-1}[\omega] + i\Sigma_{nn}[\omega])z_n[\omega] = -i \sum_{m \neq n} \Sigma_{nm}[\omega] z_m[\omega] + \sqrt{\gamma_n} \eta_n[\omega] \quad (4)$$

where $\Sigma[\omega]$ is now a matrix with elements $\Sigma_{nm}[\omega] = -i|\alpha_n \alpha_m|(\chi_c[\omega] - \chi_c^*[-\omega])$. In solving for $\Sigma[\omega]$ we continue to assume that $\omega_n \gg \gamma_n$ and that $d\omega_c/dz_n$ is a real positive number for all n so that $\alpha_n \alpha_m^* = |\alpha_n \alpha_m| = \alpha_n^* \alpha_m$. This set of equations describes a system of coupled harmonic oscillators where all of the oscillator parameters and coupling rates depend on the intra-cavity field.

Equation (4) describes the behavior of the N mechanical oscillator system, but we can better understand the behavior of our system (in which $N = 2$) by using a bright and dark state description. Specifically, we define a dark state displacement $z_d = vz_1 - uz_2$ which is a linear combination of the original, intrinsic mode displacements z_1 and z_2 with weights $u = g_1/\sqrt{g_1^2 + g_2^2}$ and $v = g_2/\sqrt{g_1^2 + g_2^2}$. The “dark” label is used because z_d is not coupled to the cavity (that is, the single-photon optomechanical coupling $g_d = 0$). On the other hand, the single-photon optomechanical coupling of the bright mode, with modal displacement $z_b = uz_1 + vz_2$, is larger than that of the original modes $g_b = \sqrt{g_1^2 + g_2^2}$.

The new modes z_b and z_d are generally not normal modes of the system, so the final ingredient in the bright/dark state description is the effective coupling between the modes $g_{bd} = uv(\xi_1 - \xi_2)$ where $\xi_n = \omega_n - i\gamma_n/2$ is the complex resonance frequency of the n^{th} mode (where $n = 1, 2$). The bright and dark states have $\xi_b = u^2 \xi_1 + v^2 \xi_2$ and $\xi_d = u^2 \xi_2 + v^2 \xi_1$. Since each mode's $Q \gg 1$, we assume

$\xi_1 - \xi_2 = \omega_1 - \omega_2$. With these assumptions, the displacement spectra $z_b[\omega]$ and $z_d[\omega]$ are

$$\begin{aligned} (\chi_b^{-1}[\omega] + i\Sigma_{bb}[\omega])z_b[\omega] &= -ig_{bd}z_d[\omega] + \sqrt{\gamma_b}\eta_b[\omega] \quad (5) \\ \chi_d^{-1}[\omega]z_d[\omega] &= -ig_{bd}z_b[\omega] + \sqrt{\gamma_d}\eta_d[\omega]. \quad (6) \end{aligned}$$

Note that the only term in these expressions that depends on the optical drive is $\Sigma_{bb}[\omega]$, which determines the optical spring and damping of the bright mode.

We use this model to fit the data in Fig. 3(a,c) and plot the resulting theoretical predictions in Fig. 3(b,d). To do this, we determine κ , Δ , and P_{in} from simultaneous measurements of the (3,3) mode (as described in Fig. 2). We then use a least-squared fit to the data in Fig. 3(a,c) to determine the remaining parameters: g_1 , g_2 , ω_1 , ω_2 , γ_1 , and γ_2 (where the subscripts 1 and 2 now label the modes (3,5) and (5,3)). This model has a small number of fit parameters and is in quantitative agreement with the data (direct comparison of the theory and data is shown in the supplemental material).

This model also provides a qualitative interpretation of the data in terms of the characteristics of the bright and dark mechanical modes. The coupling between the bright and dark states $|g_{bd}|/2\pi = 2.1$ kHz. At low P_{in} (Fig. 3(a,b)) or at high P_{in} and large detunings (near the bottom of Fig. 3(c,d)), this coupling is larger than the frequency difference between the modes $|g_{bd}| > |\omega_d - [\omega_b + \text{Re}(\Sigma_{bb}[\omega_b])]|$ because $|\omega_d - \omega_b|/2\pi = 1.4$ kHz and the optical spring effect is comparatively small. In this regime, the coupling terms $g_{bd}z_d[\omega]$ and $g_{bd}z_b[\omega]$ in equations (5) and (6), respectively, hybridize the system back into the intrinsic normal modes which independently follow the expectations of standard single-mode optomechanics.

However, when the bright mode's optical spring effect makes the coupling small in comparison to the frequency difference between the two modes $|g_{bd}| < |\omega_d - [\omega_b + \text{Re}(\Sigma_{bb}[\omega_b])]|$, then the effect of the coupling terms in equations (5) and (6) becomes small. In essence, the coupling terms are filtered by the effective mechanical susceptibilities of the bright and dark modes. Thus the coupling terms only play a role when the difference in frequencies is small relative to the strength of the coupling.

In Fig. 3(c,d) this regime of weakly-coupled bright and dark states is entered when the detuning $\Delta \gtrsim -1.5\kappa$. When the detuning $\Delta \gtrsim -0.75\kappa$ the lower-frequency state is almost entirely bright and the higher frequency state is almost entirely dark (based on the fit parameters from Fig. 3 the hybridization is 99.5%). At this point the coupling g_{bd} leads to only two noticeable effects. First, it makes the effective dark mode linewidth larger than the intrinsic linewidth of $\gamma_d/2\pi = 20$ Hz. Second, it allows the dark mode to be visible in the reflected light spectrum; otherwise this mode would be completely uncoupled from the cavity field.

The high mechanical quality factors and purely optomechanical coupling of the membrane modes make it possible to observe this hybridization in the time domain. As

shown in Fig. 4, modulation of the optical drive results in the transfer of mechanical energy between the two intrinsic mechanical modes.

This measurement starts by using a piezo to drive either the (3,5) or (5,3) mechanical mode and locking the cavity to a weak laser beam with detuning $\Delta_{\text{weak}} = -0.7\kappa$ for Fig. 4(a,b,c) and $\Delta_{\text{weak}} = -0.4\kappa$ for Fig. 4(d,e,f). For this measurement, the cavity linewidth $\kappa/2\pi = 40$ MHz. The weak laser beam is primarily used to measure the mechanical displacement, though its dynamical backaction does increase the mechanical linewidths by a factor ~ 2 . The piezo drive is turned off and a strong laser beam at detuning $\Delta_{\text{weak}} + \kappa/8$ and power P_{in} is turned on for a time τ . This pulse hybridizes the mechanical modes. After this pulse, the weak laser beam is used to determine the energy in each of the intrinsic mechanical modes. This measurement is facilitated by the separation in time scales between the 10 ms lifetimes of the intrinsic mechanical modes, the 100 μs period of the hybridization oscillations, the 140 ns period of mechanical oscillations, and the 10 ns lifetime of the optical cavity.

In Fig. 4 we plot the ratio of the final energy in each intrinsic mechanical mode after the pulse to the total initial energy as a function of τ and at different P_{in} . In Fig. 4(a,b,c) the system is initialized by driving the (5,3) mode, while in Fig. 4(d,e,f) it is initialized by driving the (3,5) mode.

The theory curves in Fig. 4 are derived from the solution to a set of differential equations describing the motion z_1 and z_2 of two linearly coupled harmonic oscillators. The coupling and oscillator parameters are taken from the $\Sigma[\omega]$ matrix in equation (4) and depend on the strength and detuning of the ‘‘strong’’ laser pulse.

In Fig. 4, some of the parameters for the theory curves are chosen manually to match the data. The values of $g_{1,2}$, $\omega_{1,2}$, and $\gamma_{1,2}$ are determined by fitting data similar to Fig. 3. The cavity linewidth κ is measured independently. A single value of Δ is chosen to fit the data in the three upper plots. P_{in} is chosen to fit the data in Fig. 4(a), and then increased by a factor of two in Fig. 4(b), and another factor of two in Fig. 4(c), in accordance with the experimental procedure. The same approach was used to choose different values of Δ and P_{in} for the lower three plots. Finally, we apply a scaling factor of 1.3 to the initial energy in the driven mode to correct for the nonlinearity of the detector. This manual choice of six parameters completely determines the theory curves in Fig. 4.

We can gain a more qualitative understanding of the data in Fig. 4 by considering the hybridization of the original modes into bright and dark modes. The pulse power used in Fig. 4 is sufficient to hybridize the system, resulting in Rabi-like oscillations between the new eigenmodes. These oscillations are suppressed on a time scale given by the optomechanically-dominated damping rate of the bright mode. This damping rate increases with increasing P_{in} . The Rabi-like oscillation frequency also increases with P_{in}

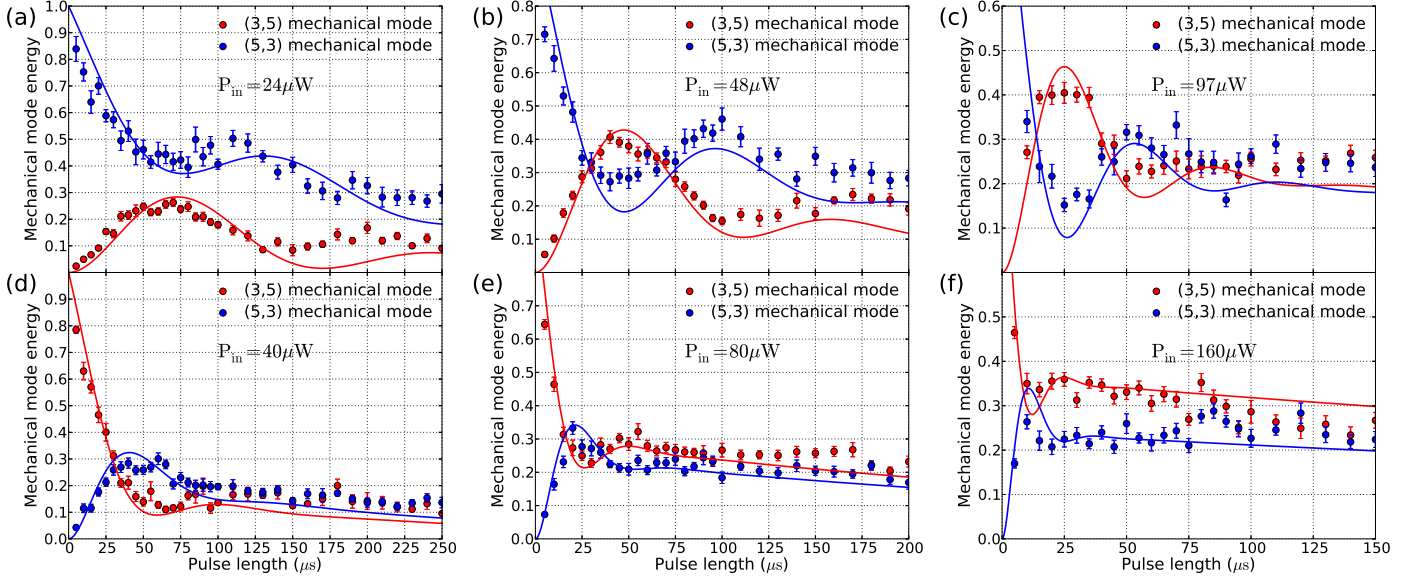


FIG. 4. The energy in each mechanical mode immediately after a hybridization pulse, plotted as a function of the pulse duration. The energy is normalized to the energy in the driven mode just before the hybridization pulse. In plots (a,b,c) the system is initialized by driving the (3,5) mode and shows the transfer of energy to the (5,3) mode. Plots (d,e,f) show the transfer of energy in the opposite direction. Solid lines are the fits described in the text, and the error bars indicate statistical uncertainties.

because the frequency splitting between the dark and bright modes is increased. At times longer than the bright mode decay, the total energy decays on a time scale given by the dark mode decay rate, while the ratio of the energy in the two modes is constant and given by the fractional contribution of each intrinsic mode to the dark mode. By optimizing the pulse power and length, we are able to transfer energy between the two intrinsic modes with an efficiency of 40% (e.g., in Fig. 4(b,c)).

This work has been supported by the DARPA/MTO ORCHID program through a grant from AFOSR.

[1] M. Aspelmeyer, T. J. Kippenberg, and F. Marquardt, arXiv:1303.0733v1 (2013).
[2] V. B. Braginsky, Y. I. Vorontsov, and K. S. Thorne, *Science* 209, 547 (1980).
[3] J. D. Thompson, B. M. Zwickl, A. M. Jayich, F. Marquardt, S. M. Girvin, and J. G. E. Harris, *Nature* 72 (2008).
[4] M. J. Hartmann and M. B. Plenio, *Phys Rev Lett* 101, 200503 (2008).
[5] P. Verlot, A. Tavernarakis, T. Briant, P.-F. Cohadon, and A. Heidmann, *Phys Rev Lett* 102, 103601 (2009).
[6] J. C. Sankey, C. Yang, B. M. Zwickl, A. M. Jayich, and J. G. E. Harris, *Nature Physics* 6, 707 (2010).
[7] M. Ludwig, K. Hammerer, and F. Marquardt, *Phys. Rev. A* 82, 012333 (2010).
[8] C. A. Regal and K. W. Lehnert, *Journal of Physics: Conference Series* 264, 012025 (2011).
[9] H. Seok, L. F. Buchmann, S. Singh, and P. Meystre, *Phys. Rev. A* 86, 063829 (2012).
[10] H. Tan, F. Bariani, G. Li, and P. Meystre,

arXiv:1302.7087v1 (2013).
[11] G. Heinrich and F. Marquardt, *Europhys. Lett.* 93, 18003 (2011).
[12] I. Wilson-Rae, N. Nooshi, W. Zwerger, and T. J. Kippenberg, *Phys. Rev. Lett.* 99, 093901 (2007).
[13] F. Marquardt, J. P. Chen, A. A. Clerk, and S. M. Girvin, *Phys. Rev. Lett.* 99, 093902 (2007).
[14] H. K. Cheung and C. K. Law, *Phys. Rev. A* 84, 023812 (2011).
[15] Q. Lin, J. Rosenberg, D. Chang, R. M. Camacho, M. Eichenfield, K. J. Vahala, and O. Painter, *Nature Photonics* 4, 236 (2010).
[16] F. Massel, S. U. Cho, J.-M. Pirkkalainen, P. J. Hakonen, T. T. Heikkilä, and M. A. Sillanpää, *Nature Communications* 3, 987 (2012).
[17] M. Zhang, G. S. Wiederhecker, S. Manipatruni, A. Barnard, P. McEuen, and M. Lipson, *Phys Rev Lett* 109, 233906 (2012).
[18] A.H. Safavi-Naeini, T.P.M. Alegre, J. Chan, M. Eichenfield, M. Winger, Q. Lin, J.T. Hill, D.E. Chang, and O. Painter, *Nature* 472, 69 (2011).
[19] D. Hunger, T. Steinmetz, Y. Colombe, C. Deutsch, T. Hänsch, and J. Reichel, *New Journal of Physics* 12, 065038 (2010).
[20] N. E. Flowers-Jacobs, S. W. Hoch, J. C. Sankey, A. Kashkanova, A. M. Jayich, C. Deutsch, J. Reichel, and J. G. E. Harris, *Appl. Phys. Lett.* 101, 221109 (2012).

Supplemental material: Optically Mediated Hybridization Between Two Mechanical Modes

A. B. Shkarin,^{1,*} N. E. Flowers-Jacobs,¹ S. W. Hoch,¹ C. Deutsch,² J. Reichel,² J. G. E. Harris^{1,3}

¹ Department of Physics, Yale University, New Haven, CT 06520, USA

² Laboratoire Kastler Brossel, ENS/UPMC-Paris 6/CNRS, F-75005 Paris, France

³ Department of Applied Physics, Yale University, New Haven, CT 06520, USA

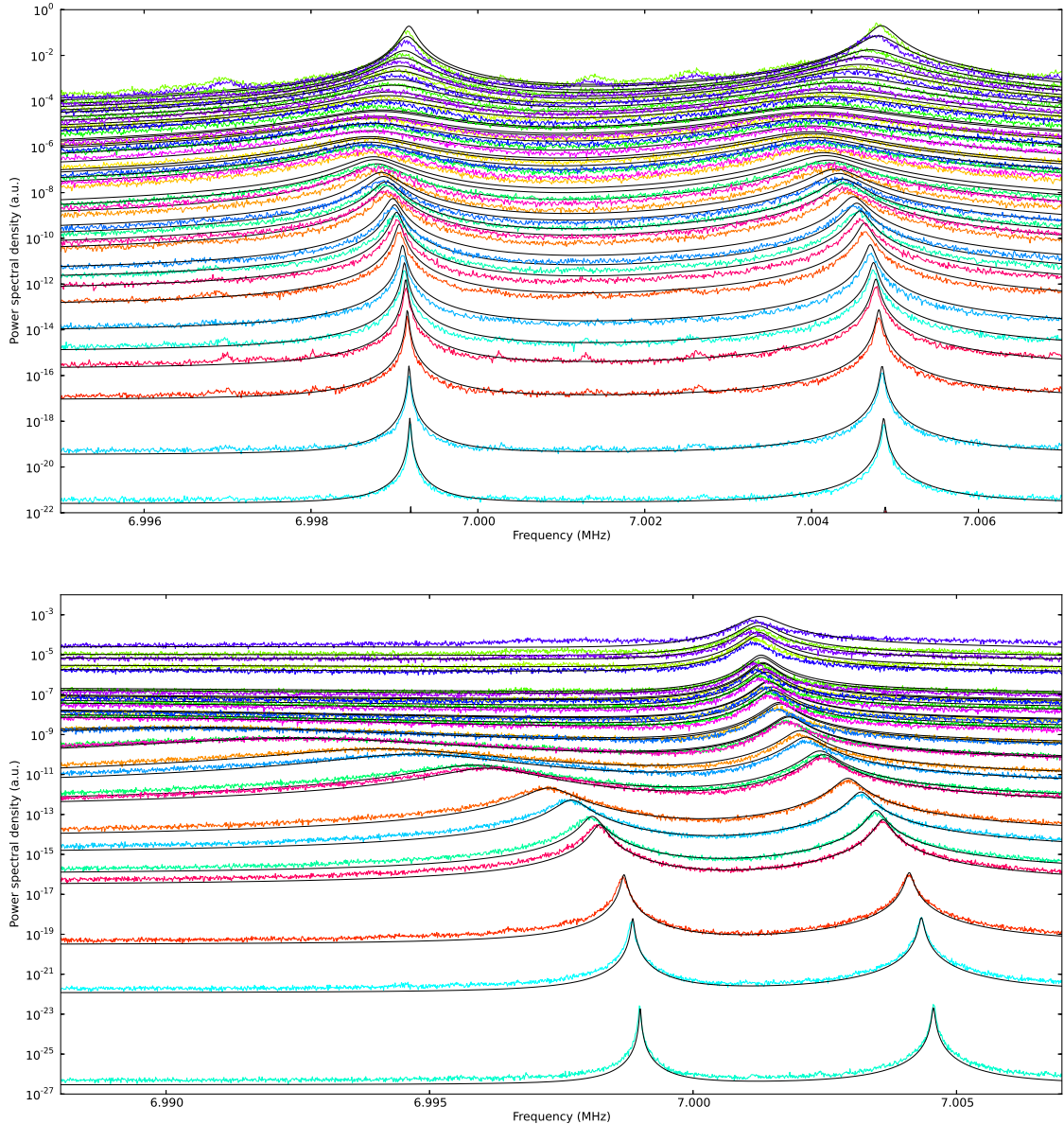


FIG. 1. Power spectral densities of reflected light showing the thermal motion of two mechanical modes. Each data set is taken at a different detuning of the incident laser beam from the cavity resonance with either $3 \mu\text{W}$ incident power (top) or $38 \mu\text{W}$ incident power (bottom). For clarity, the experimental data (color lines) and fit to theory (black lines) at each detuning are offset along the y-axis by 1 decade per MHz of detuning (that is, 1 decade per 0.05κ of detuning). The same experimental data and fits are presented as density plots in Fig. 3 of the main article; these supplemental plots are intended to facilitate a more detailed comparison of the measured power-spectral density and theoretical fits. The theory and fitting procedure are discussed in the main article.